International Journal of Bifurcation and Chaos, Vol. 17, No. 5 (2007) 1609–1622

INTERACTION OF FAST-SCALE AND SLOW-SCALE BIFURCATIONS IN CURRENT-MODE CONTROLLED DC/DC CONVERTERS

YANFENG CHEN*, CHI K. TSE† and SIU-CHUNG WONG
Department of Electronic and Information Engineering,
Hong Kong Polytechnic University, Hong Kong, P. R. China
**eeyfchen@scut.edu.cn*
†*encktse@polyu.edu.hk*

SHUI-SHENG QIU
**College of Electronic and Information Engineering,*
South China University of Technology, Guangzhou, P. R. China

Received July 13, 2006; Revised September 1, 2006

This paper investigates the interaction of fast-scale and slow-scale bifurcations in the boost converter under current-mode control operating in continuous conduction mode. Effects of varying some chosen parameters on the qualitative behaviors of the system are studied in detail. Analysis is performed to identify the different types of bifurcation. Boundaries of stable region, slow-scale bifurcation region, fast-scale bifurcation region, interacting fast and slow-scale bifurcation regions are identified.

Keywords: Bifurcation; current-mode control; fast-scale instability; slow-scale instability.

1. Introduction

The current-mode control scheme is a widely used control method for dc/dc converters, especially for the boost and buck-boost types of dc/dc converters [Redl & Sokal, 1985]. Bifurcation behaviors in dc/dc converters under current-mode control have been reported recently [Banerjee & Chakrabarty, 1998; Chan & Tse, 1997]. Generally, two distinct types of bifurcation have been identified for such circuits, namely slow-scale bifurcation and fast-scale bifurcation. The slow-scale bifurcation can be regarded as a kind of low-frequency instability which is caused by the voltage feedback loop permitting low-frequency oscillation [El Aroudi *et al.*, 1999; Tse *et al.*, 2000; Wong *et al.*, 2004]. The fast-scale bifurcation, which is caused by inner current loop instability, is often found in current-mode controlled converters, and it manifests as period-doubling in the time scale, as reported in [Iu & Tse, 2001] for parallel boost converters, [Wong *et al.*, 2006] for noise-coupled boost converters, and [Wu *et al.*, 2006] for power-factor-correction converters. The fast-scale and slow-scale bifurcations have been independently investigated as it has been generally believed that the outer voltage loop is much slower than the inner current loop and the two loops can be considered noninteracting. As a result, slow-scale bifurcation and fast-scale bifurcation have been studied separately.

In the usual current-mode controlled dc/dc converter, the outer voltage feedback loop provides the necessary current reference for the inner current loop. The outer voltage feedback loop contains typically a proportional-integral controller and hence has a low-pass characteristic, whereas the inner current loop is as fast as the switching frequency. The

instability in the outer voltage loop is a slow-scale phenomenon, whereas the instability of the inner current loop is a fast-scale one. Moreover, the two loops actually interact with each other as the current reference used to program the inductor current in the inner current loop is produced by the outer voltage loop. Therefore, the two mechanisms responsible for the fast-scale and slow-scale bifurcations can actually interact with each other, leading to possible interacting fast-scale and slow-scale bifurcations. Our objective in this paper is to study such interaction and to identify the boundaries of stable region, slow-scale bifurcation region, fast-scale bifurcation region, and the interacting region in terms of some chosen parameters.

As dc/dc converters may operate in continuous-conduction-mode (CCM) or discontinuous-conduction-mode (DCM), depending upon the parameter choice and the dynamical status, it is possible that such systems may toggle between the two operating modes in a rather complex manner. To facilitate analysis, the converter parameters are chosen such that CCM is the default operating mode. Thus, *normal stable operation* refers to the stable period-1 operation in CCM. Subsequently, *instability* refers to operation that is *not* the normal stable operation, and *bifurcation* refers to the change from one type of operation to another.

This paper is organized as follows. In Sec. 2, we will review the operation of the boost converter under peak-current-mode (PCM) control. In Sec. 3, we will present some typical waveforms of normal stable operation, slow-scale bifurcation, fast-scale bifurcation, interacting fast-scale and slow-scale bifurcation, and "saturated" unstable operation (in which the duty cycle saturates to 100% as the error amplifier in the voltage feedback loop saturates). Analysis of these bifurcation phenomena will be presented in Sec. 4, which is based on tracking the movements of the eigenvalues of the Jacobians evaluated at the appropriate operating states [Guckenheimer & Holmes, 1983]. In Sec. 5 we will present the boundaries of various operations in some chosen parameter spaces by computer simulations of the actual system and compare them with those obtained by the analytical method derived in Sec. 4. Here, the slope of inductor current and the compensation slope in the inner current loop are selected as the parameters for fast-scale bifurcation, whereas the feedback gain and time constant in the outer voltage loop are selected as the parameters for slow-scale bifurcation. Finally we conclude this paper in Sec. 6.

2. Operation of the Current-Mode Controlled Boost Converter

The closed-loop current-mode controlled boost converter under study is shown in Fig. 1(a). The system has an outer voltage loop and an inner current loop. The voltage loop consists of an error amplifier (EA) and a compensation network, the output of which provides the reference for the inner current loop. The inner current loop consists of a current transformer and a current sense amplifier

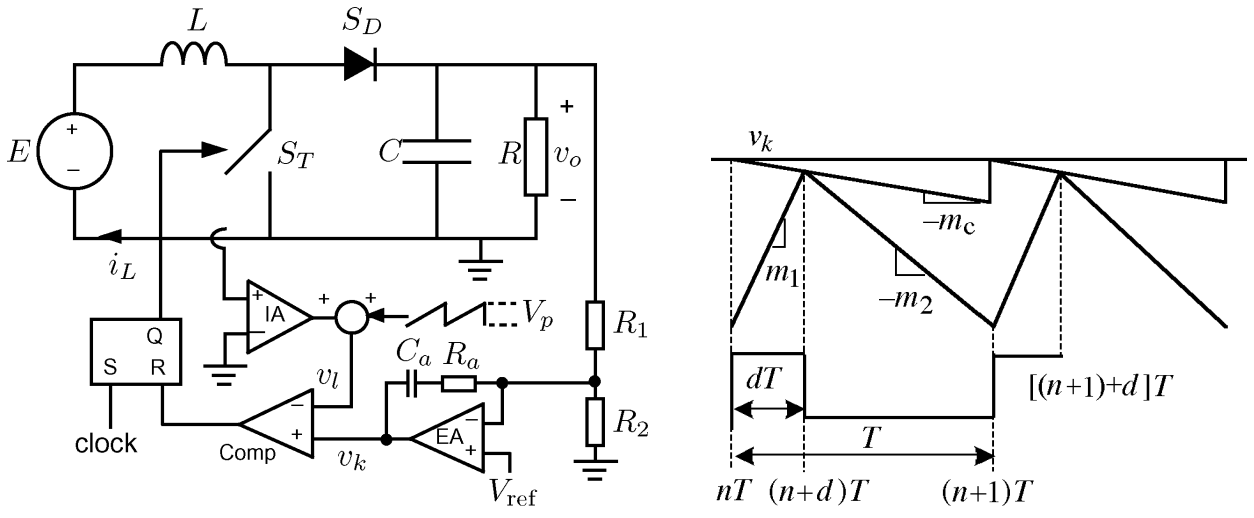

(a) (b)

Fig. 1. (a) Boost converter under current-mode control; (b) typical waveforms.

(IA). A compensation ramp is added to stabilize the converter if a wide range of output voltage is required [Wong *et al.*, 2004]. The output of the current loop is then connected to the inputs of the comparator whose output is used to reset a flip-flop latch to give a pulse-width modulated waveform to control switch S_T. The operation can be briefly described as follows. The flip-flop latch is set periodically by the clock signal, turning on the switch S_T. Then, the inductor current i_L goes up linearly, and is compared with a reference level, which is equal to the output of the error amplifier of the voltage loop minus the compensation ramp signal. When the peak inductor current reaches the reference level, the output of the comparator resets the flip-flop, thereby turning off the switch. When the switch is off, the inductor current falls almost linearly if the output capacitor is sufficiently large. The cycle repeats when the flip-flop is set again by the clock. Typical waveforms of the converter operating in CCM are shown in Fig. 1(b), where m_c is the slope of the compensation ramp signal, and m_1 and m_2 are the rising and falling slopes of the inductor current with the switch on and off respectively.

3. A Glimpse at Bifurcation Behavior

We begin with a series of typical waveforms from exact cycle-by-cycle computer simulations to show some possible bifurcation behaviors in this system. As our aim is to study the interaction of fast-scale and slow-scale bifurcations, the unstable operations associated with "saturation" of control signals (typically manifested as saturation of the duty cycle) will not be examined because these operations occur well beyond the boundaries of the first fast-scale or slow-scale bifurcations.[1] The main parameters affecting fast-scale bifurcations are the rising slope of the inductor current m_1, and the compensation slope m_c, whereas those affecting slow-scale bifurcations are the voltage feedback gain g and time constant τ_f, as studied previously in [Wong *et al.*, 2004]. To facilitate simulation study, we choose parameter values as listed in Table 1.

For a certain range of parameters, normal periodic operation, slow-scale bifurcation, fast-scale bifurcations, coexisting fast and slow-scale bifurcation, and "saturated" operation (border collision) can be observed. Typical waveforms are shown in Figs. 2–4. Here, $E = 6.1877\,\text{V}$ and $R = 10.78\,\Omega$ are fixed, and m_1 ($m_1 = E/L$) is changed by varying the inductance L, thereby ensuring that the system has a fixed duty cycle. Consistent with usual understanding, we can see from these waveforms that slow-scale bifurcations can be eliminated by increasing the feedback gain or time constant, and that fast-scale bifurcations can be eliminated by increasing m_c, or decreasing m_1 via increasing L.

Table 1. Circuit parameters for simulation study.

Component/Parameter	Value
Input voltage E	3–20 V
Inductance L	120–195 μH
Capacitance C	2000 μF
Load resistance R	3–20 Ω
Switching frequency f_s	25 kHz
Reference output voltage V_{ref}	1.8 V
Voltage divider R_1, R_2	47.5 kΩ, 2.5 kΩ
Compensation network R_a, C_a	72.3 kΩ, 0.23 μF
Compensation ramp V_p	0.25 A
Inductance current sampling gain M	0.082

4. Bifurcation Analysis of the Closed-Loop Current-Mode Controlled Boost Converter

From the foregoing simulation studies, we have briefly observed slow-scale bifurcation, fast-scale bifurcation and interacting bifurcation in certain parameter ranges. In this section we will analyze these bifurcations by making use of a suitable discrete-time model. We will first derive the exact discrete-time model that describes the dynamics of the system, and investigate the dynamical behavior by examining the movements of the characteristic multipliers (eigenvalues) of the Jacobians as some chosen parameters are varied [Guckenheimer & Holmes, 1983].

4.1. *Derivation of state equations*

The boost converter described above can be regarded as a variable structure that toggles its topology according to the states of the switches.

[1]By "first" fast-scale or slow-scale bifurcations, we mean those bifurcations adjacent to the normal operation. This type of bifurcation is the only practically meaningful type of bifurcation as it gives the mechanism through which the system loses stability.

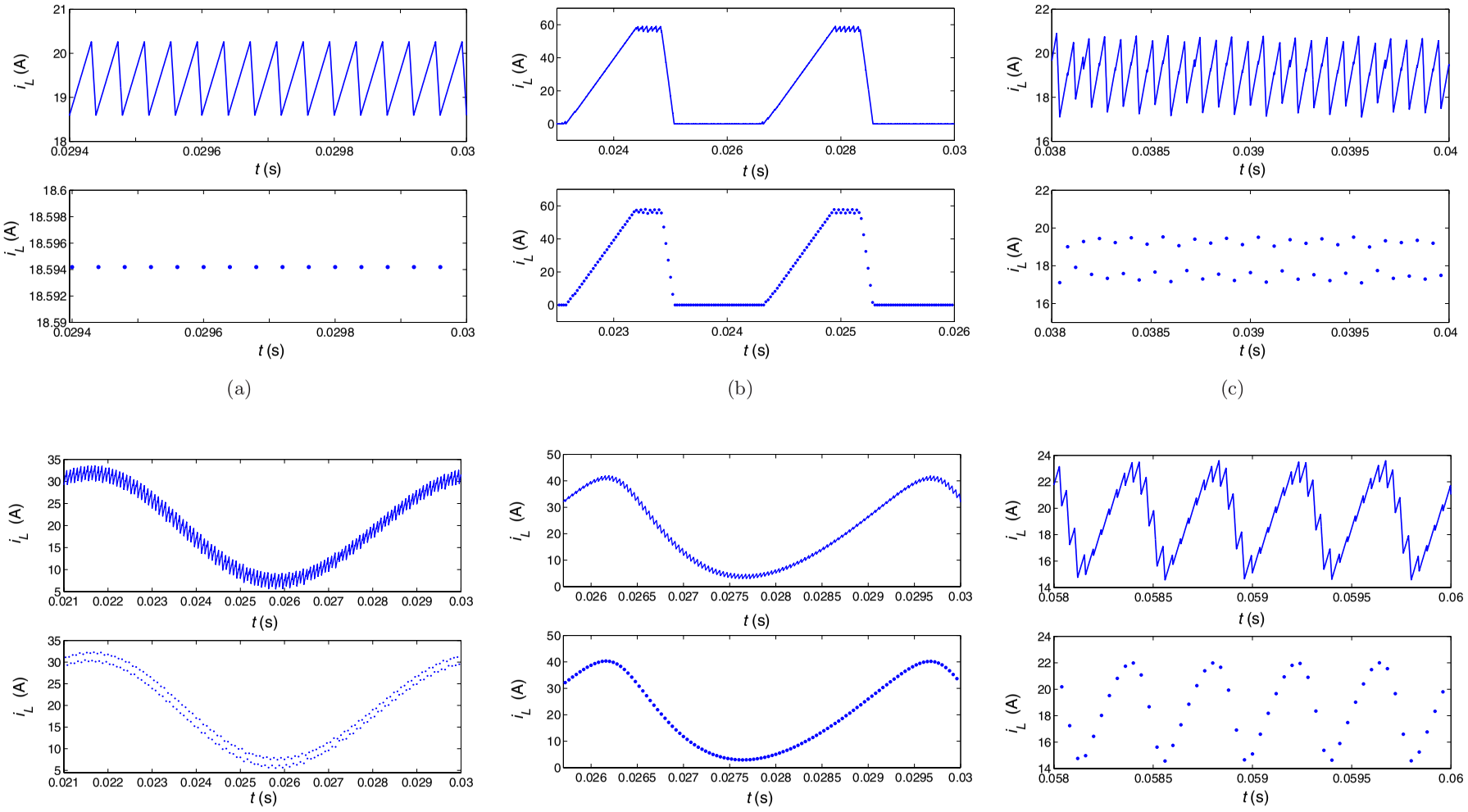

Fig. 2. Simulated behaviors for different feedback gain $g = R_a/R_1$ and time constant $\tau_f = R_1 C_a$, with $1/m_1 = 19.835 \times 10^{-6}$ s/A, $m_c = 6.25 \times 10^3$ A/s. Upper trace: actual waveforms, lower trace: sampled-data waveforms. (a) Stable periodic operation with $g = 1.522$ and $\tau_f = 0.5225$ ms, (b) saturated operation with $g = 1.522$ and $\tau_f = 0.475$ ms, (c) fast-scale bifurcation with $g = 0.1$ and $\tau_f = 10.925$ ms, (d) coexisting (interacting) fast and slow-scale bifurcation with $g = 0.1$ and $\tau_f = 2.09$ ms, (e) slow-scale bifurcation $g = 0.8$ and $\tau_f = 0.492$ ms, (f) slow-scale bifurcation with $g = 2.4$ and $\tau_f = 7.125$ ms.

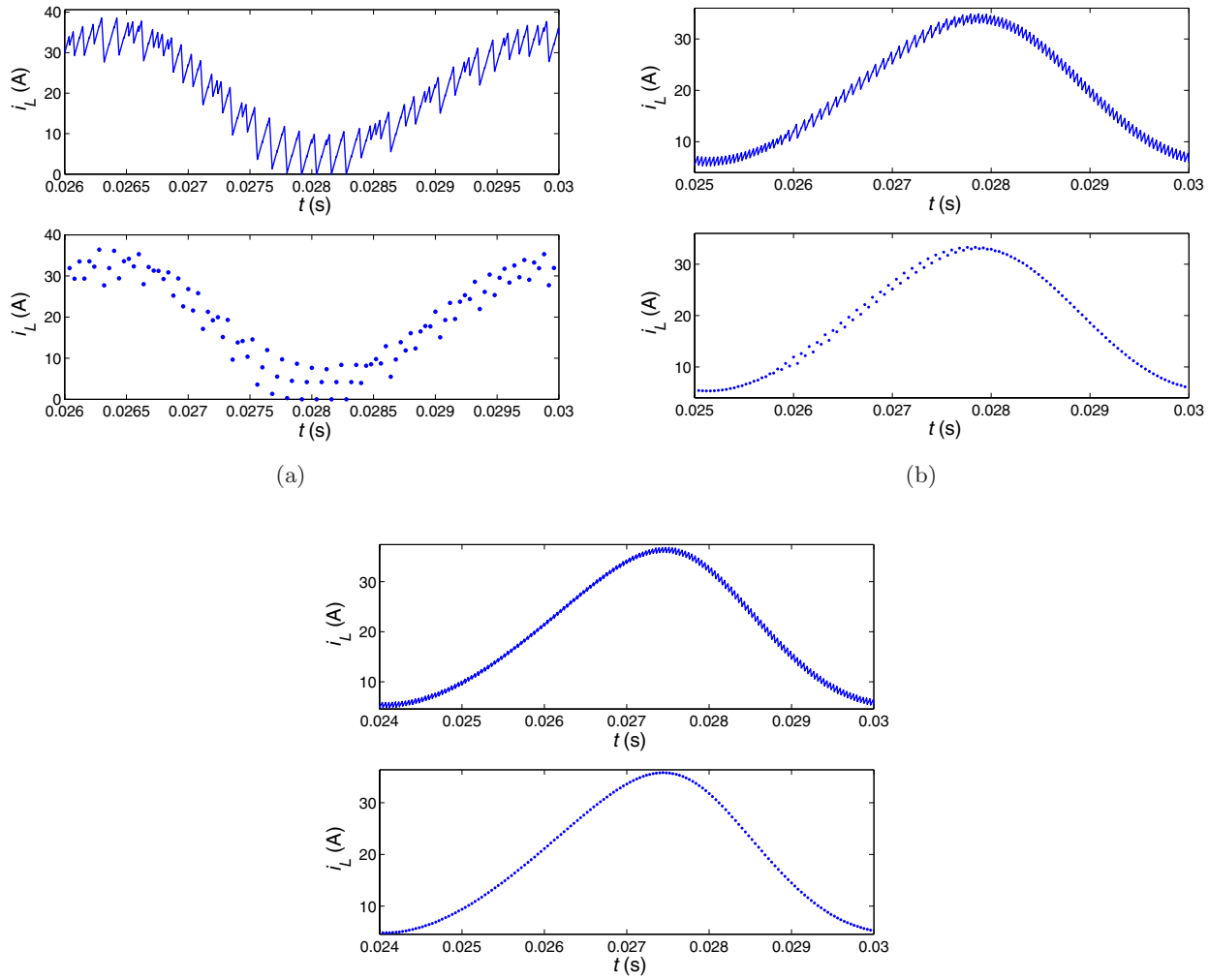

Fig. 3. Simulated behaviors for different values of m_1 and τ_f, with $g = 0.4$ and $m_c = 6.25 \times 10^3$ A/s. (a) Coexisting (interacting) fast and slow-scale bifurcations with $1/m_1 = 9 \times 10^{-6}$ s/A and $\tau_f = 0.362$ ms, (b) coexisting (interacting) fast and slow-scale bifurcations with $1/m_1 = 19.835 \times 10^{-6}$ s/A and $\tau_f = 0.8265$ ms, (c) slow-scale bifurcation with $1/m_1 = 31.514 \times 10^{-6}$ s/A and $\tau_f = 1.3538$ ms.

When operating in CCM, two switch states can be identified.

State 1: switch S_T on and diode S_D off.
State 2: switch S_T off and diode S_D on.

The two switch states toggle periodically in the steady state. We assume that the circuit takes state 1 for $nT_s \leq t < (n+d)T_s$, and state 2 for $(n+d)T_s \leq t < (n+1)T_s$, where n is an integer, T_s is the switching period, and d is the duty cycle, which is defined as the ratio of the turn-on time of switch S_T to the switching period T_s. In a closed-loop converter system, d is usually a function of the system's state variables, as will be discussed in a later section.

As shown in Fig. 1(a), the compensator used here is a first-order PI controller. In addition to the two state variables chosen from the converter (i.e. inductor current i_L and output voltage v_o), the voltage across the compensation capacitor, v_a, can be described by the following state equation:

$$\frac{dv_a}{dt} = \frac{v_o}{\tau_f} - \frac{k_d V_{\text{ref}}}{\tau_f} \tag{1}$$

where V_{ref} is the reference output voltage, $k_d = (R_1 + R_2)/R_2$ is the ratio of the voltage divider, and $\tau_f = R_1 C_a$ denotes the time constant of the voltage feedback loop. The system is thus third-order, with the possible choice of state vector as

$$x = [i_L \quad v_o \quad v_a]^T \tag{2}$$

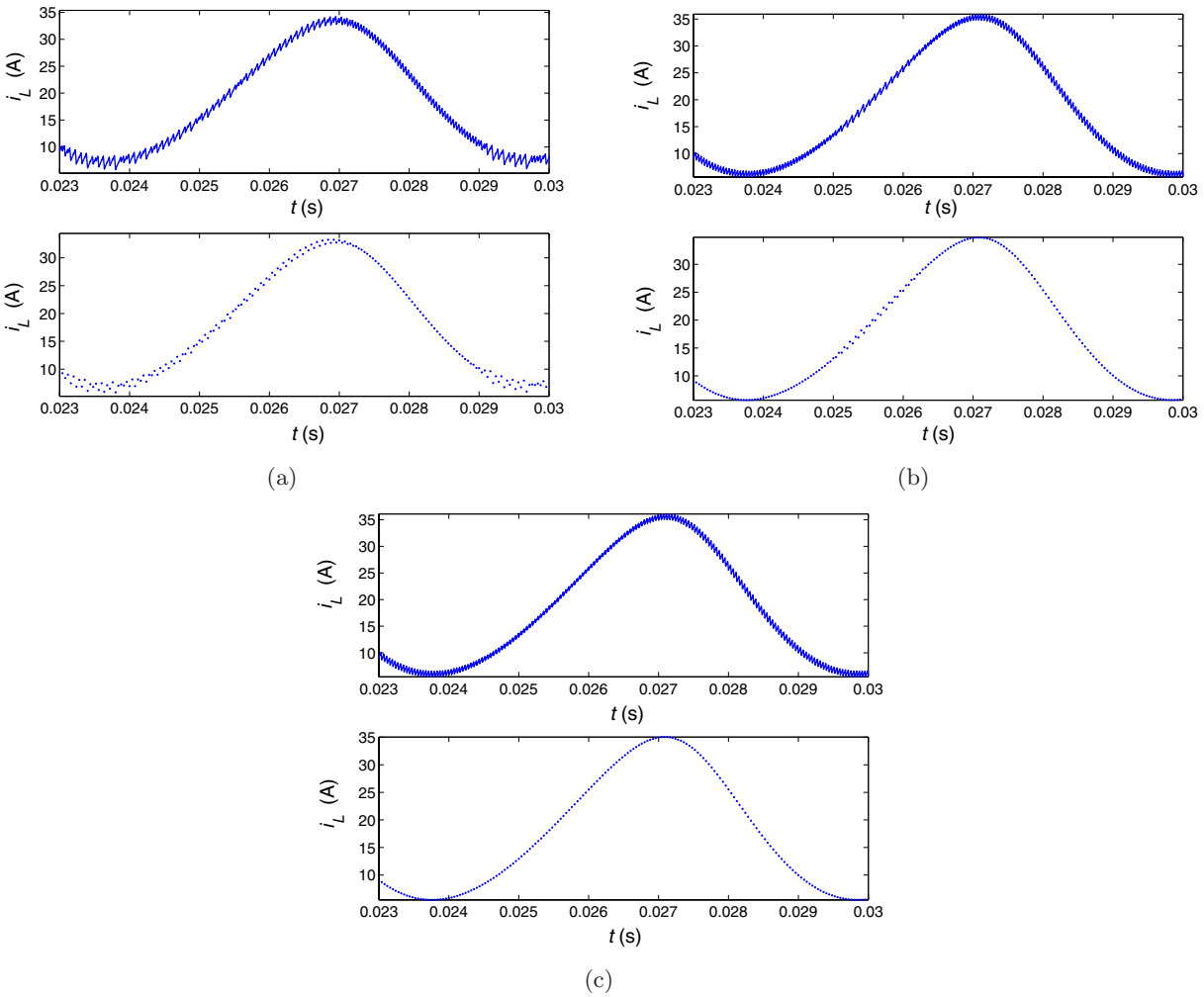

Fig. 4. Simulated behaviors for different values of m_c, with $g = 0.4$, $\tau_f = 1.3253\,\text{ms}$, and $1/m_1 = 31.514 \times 10^{-6}\,\text{s/A}$. (a) Coexisting (interacting) fast and slow-scale bifurcations with $m_c = 2.825 \times 10^3\,\text{A/s}$, (b) critical coexisting (interacting) fast and slow-scale bifurcations with $m_c = 3.825 \times 10^3\,\text{A/s}$, (c) slow-scale bifurcations with $m_c = 4.0 \times 10^3\,\text{A/s}$.

where superscript T denotes matrix transposition. Thus, the system operating in CCM can be described by the following state equations:

$$\begin{aligned} \dot{x} &= A_1 x + B_1 E \quad \text{for } nT_s \le t < (n+d)T_s \\ \dot{x} &= A_2 x + B_2 E \quad \text{for } (n+d)T_s \le t < (n+d)T_s, \end{aligned} \tag{3}$$

where E is the input voltage, and the A's and B's for this current-mode controlled boost converter are given by

$$A_1 = \begin{bmatrix} 0 & 0 & 0 \\ 0 & -\dfrac{1}{RC} & 0 \\ 0 & \dfrac{1}{\tau_f} & 0 \end{bmatrix}, \quad A_2 = \begin{bmatrix} 0 & -\dfrac{1}{L} & 0 \\ \dfrac{1}{C} & -\dfrac{1}{RC} & 0 \\ 0 & \dfrac{1}{\tau_f} & 0 \end{bmatrix}, \tag{4}$$

$$B_1 = B_2 = \begin{bmatrix} \dfrac{1}{L} \\ 0 \\ \dfrac{k_d V_{\text{ref}}}{\tau_f E} \end{bmatrix}. \tag{5}$$

4.2. *Derivation of the discrete-time map*

In this subsection we attempt to derive a discrete-time map that describes the dynamics of the current-mode controlled boost converter system with a PI controlled voltage feedback loop, as shown in Fig. 1. The form of the discrete-time map we aim to get is

$$x_{n+1} = f(x_n) \tag{6}$$

where subscript n denotes the value at the beginning of the nth cycle, i.e. $x_n = x(nT)$. Note that for the closed-loop system, d_n should not appear explicitly in the state equation because it is related to x_n via a feedback function.

As mentioned above, the state equation for the circuit in any switch state can be written in the form of a linear differential equation, i.e. $\dot{x} = A_j x + B_j E$, where $j = 1, 2$. At the sampling instant, i.e. $t = nT_s$, switch S_T is turned on and the system enters state 1. At $t = t_s = (n + d)T_s$, S_T is turned off, and the system goes to state 2.

Using a successive substitution method, the value of x at the end of the nth cycle, i.e. x_{n+1}, can be expressed as

$$\begin{aligned} x_{n+1} = {} & \Phi_2((1-d_n)T_s)(\Phi_1(d_nT_s)x_n \\ & + A_1^{-1}(\Phi_1(d_nT_s) - \mathbf{1})B_1E) \\ & + A_2^{-1}(\Phi_2((1-d_n)T_s) - \mathbf{1})B_2E \end{aligned} \quad (7)$$

where $\mathbf{1}$ is the unit matrix and $\Phi_j(\xi)$ is the transition matrix corresponding to A_j and is given by

$$\Phi_j(\xi) = e^{A_j\xi} = \mathbf{1} + \sum_{k=1}^{\infty} \frac{1}{k!} A_j^k \xi^k, \quad \text{for } j = 1, 2. \quad (8)$$

To complete the derivation, we have to find the feedback relation that connects the duty cycle d_n and the state variables x_n. In the closed-loop system, d_n is controlled via the control signal v_k, which is derived from the output voltage via a PI compensation network, i.e.

$$v_k = V_{\text{ref}}(1 + gk_d) - gv_o - v_a \quad (9)$$

where $g = R_a/R_1$ is the DC gain of the feedback voltage loop. Also, from (2), the control signal v_k can be expressed as a linear function of x, i.e.

$$v_k = k_0 + k_1 x \quad (10)$$

where $k_0 = V_{\text{ref}}(1 + gk_d)$ and $k_1 = [0 \quad -g \quad -1]$.

Suppose v_l is the sensed inductor current analog, i.e. $v_l = Mi_L$, where M is the current sampling gain. During state 1, i_L rises linearly, and so does v_l. When v_l reaches the control signal level, i.e. $v_l = v_k$, switch S_T is turned off. From (10), we may define a switching function $s(x_n, d_n)$ as

$$\begin{aligned} s(x_n, d_n) & \stackrel{\text{def}}{=} v_k(t_s) - Mi_L(t_s) - m_c d_n T_s \\ & = k_0 + k_1 x(t_s) - Mi_L(t_s) - m_c d_n T_s \\ & = k_0 + k_1 x(t_s) - Mi_L n \\ & \quad - (Mm_1 + m_c)d_n T_s \end{aligned} \quad (11)$$

where k_0, k_1 are as defined before, and $m_1 = E/L$ is the rising slope of the inductor current. Obviously, at $t = t_s$, we have $s(x_n, d_n) = 0$, and S_T is turned off. In other words, $s(.) = 0$ defines the condition for the system to go from state 1 to state 2. Substituting $x(t_s)$ in (11), we get

$$\begin{aligned} s(x_n, d_n) = {} & k_0 + (k_1\Phi_1(d_nT_s) + k_2)x_n \\ & + k_1A_1^{-1}(\Phi_1(d_nT_s) - \mathbf{1})B_1E \\ & - (Mm_1 + m_c)d_nT_s \end{aligned} \quad (12)$$

where $k_2 = [-M \quad 0 \quad 0]$, and d_n can be expressed as

$$d_n = \frac{\begin{aligned} & k_0 + k_1(\Phi_1(d_nT_s) + k_2)x_n \\ & + k_1A_1^{-1}(\Phi_1(d_nT_s) - \mathbf{1})B_1E) \end{aligned}}{(Mm_1 + m_c)T_s}. \quad (13)$$

We note that (13) is transcendental, and can only be solved numerically. Combining with (7), we have the nonlinear discrete-time model for the closed-loop system.

4.3. *Derivation of the Jacobian*

In this section, we aim to find the Jacobian for any given equilibrium state. The essence of using a Jacobian in the analysis of dynamical systems lies in the capture of the dynamics in the small neighborhood of the equilibrium point or orbit. Then, by inspecting the eigenvalues of the Jacobian, we are able to determine the stability of the equilibrium state. Furthermore, by studying the movement of the eigenvalues (also called *characteristic multipliers* for discrete-time systems) of the Jacobian under the variation of selected parameters, stability information such as the occurrence of bifurcations and boundaries of operating regimes can be identified.

We now begin with finding the equilibrium point X_Q and the corresponding duty cycle D_Q of the system, i.e. the steady-state solution. Obviously, the desired steady-state solution can be solved by putting $x_n = X_Q$ in (13). As the system is nonlinear, numerical procedures have to be used for finding X_Q. By using the definition of the equilibrium point $x_{n+1} = x_n = X_Q$ in (7), X_Q can be explicitly expressed as a function of D_Q (steady-state value of d_n). Then, from (13), D_Q can be solved numerically and hence X_Q can be obtained. The Jacobian of the discrete-time map evaluated at the equilibrium point can be written as

$$J(X_Q) = \frac{\partial f}{\partial x_n} - \frac{\partial f}{\partial d_n}\left(\frac{\partial s}{\partial d_n}\right)^{-1}\left(\frac{\partial s}{\partial x_n}\right)\Bigg|_{x_n = X_Q}. \quad (14)$$

Using (7) and (12), we can find all the derivatives in (14). First, $\partial f/\partial x_n$ can be found from (7), i.e.

$$\frac{\partial f}{\partial x_n} = \Phi_2((1-d_n)T_s)\Phi_1((d_n)T_s). \tag{15}$$

Also, direct differentiation gives $\partial f/\partial d_n$ as

$$\begin{aligned}\frac{\partial f}{\partial d_n} &= T_s\Phi_2((1-d_n)T_s)[\Phi_1(d_nT_s)(A_1x_n + B_1E) \\ &\quad - A_2\Phi_1(d_nT_s)x_n - A_2(\Phi_1(d_nT_s) \\ &\quad - \mathbf{1})A_1^{-1}B_1E - B_2E].\end{aligned} \tag{16}$$

From (12), we obtain $\partial s/\partial x_n$ readily as

$$\frac{\partial s}{\partial x_n} = k_1\Phi_1(d_nT_s) + k_2. \tag{17}$$

Again, by direct differentiation, we get

$$\begin{aligned}\frac{\partial s}{\partial d_n} &= k_1T_s\Phi_1(d_nT_s)(A_1x_n + B_1E) \\ &\quad - (Mm_1 + m_c)T_s.\end{aligned} \tag{18}$$

Finally, putting all the derivatives into (14) gives an expression of $J(X_Q)$. Numerical algorithms can now be developed for computing $J(X_Q)$ and hence the eigenvalues, as will be shown in the next subsection.

4.4. *Interacting bifurcations*

Bifurcation and stability information can be obtained by examining the eigenvalues (characteristic multipliers) of the Jacobian derived in the foregoing. In particular, we are interested in the movement of the eigenvalues as some chosen parameters are varied. This information essentially reveals the bifurcation phenomena and the way in which variation of parameters affect the operation of the system. First, we need to compute the eigenvalues, which can be accomplished by solving the following polynomial equation in λ:

$$\det[\lambda\mathbf{1} - J(X_Q)] = 0 \tag{19}$$

where $J(X_Q)$ is the Jacobian found previously. We will pay special attention to the movement of the eigenvalues as some chosen parameters are varied. Specifically, if all eigenvalues of the Jacobian are inside the unit circle, the equilibrium state about which the Jacobian has been evaluated is stable. Any crossing from the interior of the unit circle to the exterior indicates a loss of stability of the equilibrium state, i.e. a bifurcation occurs at the point of crossing. When a pair of complex eigenvalues move out of the unit circle, the system undergoes a slow-scale bifurcation, and when a negative real eigenvalue moves out of the unit circle (i.e. crossing -1), a fast-scale period-doubling bifurcation occurs [Stjepan *et al.*, 1991]. Moreover, if both conditions are satisfied, some interaction of these two kinds of bifurcation is expected. Thus, we may identify the critical values of the bifurcation parameters as those values where the loci of the eigenvalues cross the unit circle.

Using (14) and (19), we can generate loci of the eigenvalues numerically. As we are interested in the loci of the eigenvalues corresponding to interacting bifurcations, we will systematically examine the loci under variation of different sets of parameters. As a quick overview, we first vary E and L/E and track the loci of the eigenvalues, as shown in Fig. 5. Here, all parameters, except L, R and E, are chosen as listed in Table 1. In Fig. 5(a), $L = 195\,\mu$H and $R = 10.78\,\Omega$, with E being varied from 6.1466 V to 6.5758 V. The movement of the complex eigenvalues across the unit circle at $E = 6.40332$ V indicates a slow-scale bifurcation, which is consistent with the simulated result shown in Fig. 8(a). In Fig. 5(b), $E = 6.1877$ V and $R = 10.78\,\Omega$ and L/E is varying from 12.87×10^{-6} s/A to 34.67×10^{-6} s/A. The locus of the negative real eigenvalue crosses the unit circle at $L/E = 13.639 \times 10^{-6}$ s/A (while the complex eigenvalues stay inside the unit circle), indicating that a fast-scale bifurcation occurs. Also, as the complex eigenvalues cross the unit circle at $L/E = 30.49 \times 10^{-6}$ s/A (while the real eigenvalue stays inside the unit circle), a slow-scale bifurcation occurs. In both cases, the critical values are close to the simulated results shown earlier in Fig. 8(b). Under these conditions, there is no interacting bifurcation.

Now we focus on the loci when g, τ_f, L/E and m_c are varied. Results are shown in Tables 2–5, and also illustrated in Figs. 6 and 7. In summary, the system's behavior can be identified according to the movement of the eigenvalues of the Jacobian:

(1) All the eigenvalues inside the unit circle indicates stable operation.
(2) Slow-scale bifurcation occurs when a pair of complex eigenvalues move out of the unit circle while other eigenvalues stay inside the unit circle.
(3) Fast-scale bifurcation occurs when a negative real eigenvalue moves out of the unit circle while all other eigenvalues stay inside the unit circle.

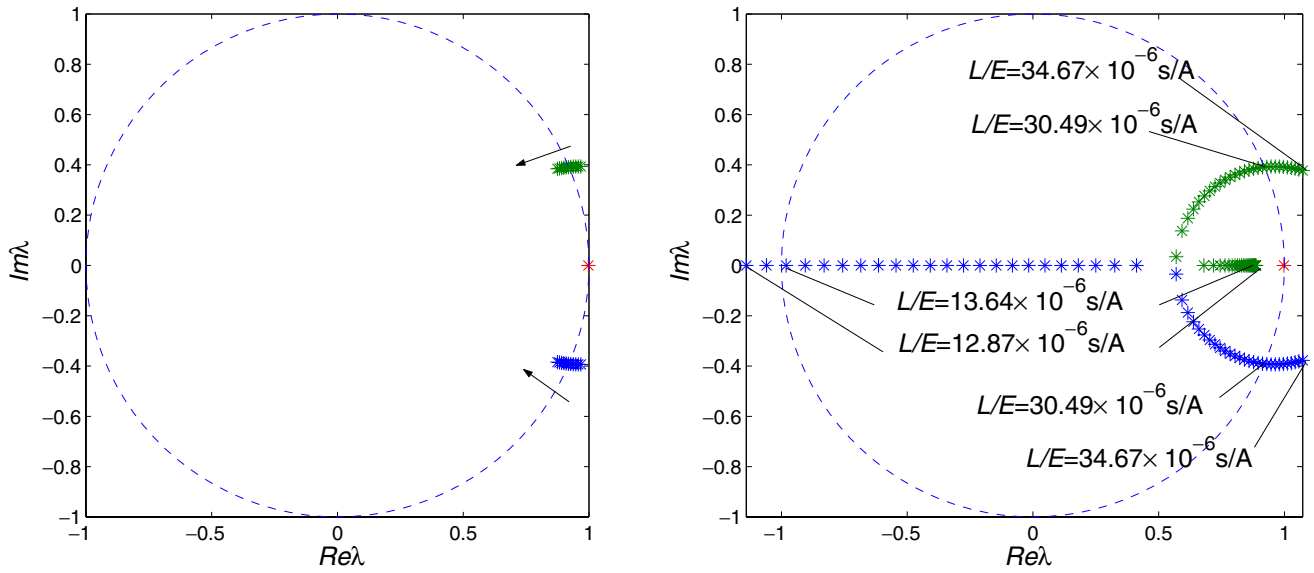

(a) (b)

Fig. 5. Loci of eigenvalues for relatively large $g = 1.522$ and $\tau_f = 10.925\,\text{ms}$ under (a) varying E for $L = 195\,\mu\text{H}$ and $R = 10.78\,\Omega$; (b) varying L/E for $E = 6.1877\,\text{V}$ and $R = 10.78\,\Omega$. Arrows indicate the direction of movement of the eigenvalues as the chosen parameters are increased.

Table 2. Eigenvalues for different values of τ_f.

τ_f (ms)	Eigenvalues	Modulus (Complex Pair)	Remarks
0.16530	$1.0455 \pm j0.10435,\ -1.0033$	1.0507	"saturated" unstable
0.31407	$1.0172 \pm j0.079517,\ -1.0305$	1.0203	"saturated" unstable
0.61161	$1.0026 \pm j0.057766,\ -1.0455$	1.0042	"saturated" unstable
0.80997	$0.9989 \pm j0.050127,\ -1.0493$	1.0001	interacting bifurcation
1.05792	$0.9962 \pm j0.043641,\ -1.0522$	0.9972	fast-scale bifurcation
1.20669	$0.9951 \pm j0.040702,\ -1.0533$	0.9960	fast-scale bifurcation
1.65300	$0.9931 \pm j0.034295,\ -1.0555$	0.9937	fast-scale bifurcation

Table 3. Eigenvalues for different values of g.

g	Eigenvalues	Modulus (Complex Pair)	Remarks
0.1	$1.0054 \pm j0.045937,\ -1.2346$	1.0064	"saturated" unstable
0.2	$1.0033 \pm j0.04718,\ -1.1813$	1.0045	"saturated" unstable
0.3	$1.0011 \pm j0.048407,\ -1.1167$	1.0023	"saturated" unstable
0.4	$0.99863 \pm j0.049611,\ -1.0496$	0.9999	interacting bifurcation
0.5	$0.9959 \pm j0.050774,\ -0.97975$	0.9972	stable
0.6	$0.99286 \pm j0.051875,\ -0.90699$	0.9942	stable
0.7	$0.98946 \pm j0.052883,\ -0.83107$	0.9909	stable

(4) Interacting fast and slow-scale bifurcation occurs when a negative real eigenvalue and a pair of complex eigenvalues move out of the unit circle at the same time.
(5) Complex border collision bifurcation involving "saturated" operation occurs when some eigenvalues leap out of the unit circle.

The above analytical procedure is useful for identifying the behavior for a particular set of parameters (at a particular point in the parameter space). However, in order to be useful for engineering applications, it would be imperative to know the structure of the parameter space with respect to the various operations and bifurcation

Table 4. Eigenvalues for different values of L/E.

L/E ($\times 10^{-6}$ s/A)	Eigenvalues	Modulus (Complex Pair)	Remarks
9.00	$0.99269 \pm j0.046400,\ -2.3270$	0.9938	fast-scale bifurcation
12.833	$0.99465 \pm j0.047575,\ -1.7594$	0.9958	fast-scale bifurcation
16.667	$0.99676 \pm j0.048710,\ -1.3312$	0.9979	fast-scale bifurcation
19.925	$0.99868 \pm j0.049636,\ -1.04237$	0.9999	interacting bifurcation
24.333	$1.0015 \pm j0.050809,\ -0.72956$	1.0028	"saturated" unstable
28.167	$1.0042 \pm j0.051733,\ -0.51107$	1.0055	"saturated" unstable
32.000	$1.0071 \pm j0.052537,\ -0.32969$	1.0085	"saturated" unstable

Table 5. Eigenvalues for different values of m_c.

m_c ($\times 10^3$ A/s)	Eigenvalues	Modulus (Complex Pair)	Remarks
3.4425	$0.99971 \pm j0.014857,\ -1.5014$	0.9998	interacting bifurcation
3.8250	$0.99972 \pm j0.014857,\ -1.3525$	0.9998	interacting bifurcation
4.2075	$0.99972 \pm j0.014857,\ -1.2203$	0.9998	interacting bifurcation
4.5900	$0.99972 \pm j0.014856,\ -1.1021$	0.9998	interacting bifurcation
4.9572	$0.99972 \pm j0.014856,\ -1.0000$	0.9998	interacting bifurcation
5.3350	$0.99972 \pm j0.014856,\ -0.9000$	0.9998	slow-scale bifurcation
5.7375	$0.99972 \pm j0.014856,\ -0.8128$	0.9998	slow-scale bifurcation

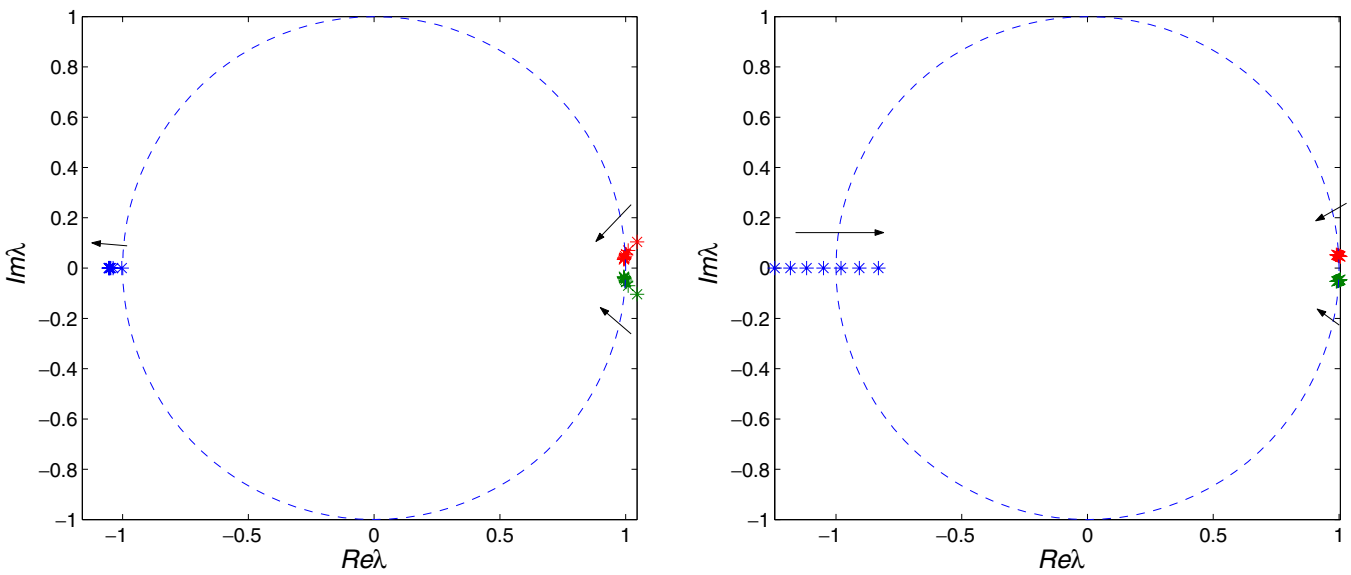

(a) (b)

Fig. 6. Loci of eigenvalues for $E = 6.1877\,\mathrm{V}$, $R = 10.78\,\Omega$ under (a) varying τ_f when $1/m_1 = 19.835 \times 10^{-6}\,\mathrm{s/A}$, $g = 0.4$, (b) varying g when $1/m_1 = 19.835 \times 10^{-6}\,\mathrm{s/A}$ and $\tau_f = 0.8265\,\mathrm{ms}$. Arrows indicate the direction of movement of the eigenvalues as the chosen parameters are increased.

scenarios. Such information allows the engineers to know how "far" or "close" the system is from the boundary of instability and in what way the system would lose stability should the parameters vary in some given directions. In Sec. 5, we will provide extensive simulations, alongside with analytical results, to illustrate the boundaries of slow-scale bifurcation, fast-scale bifurcation and interacting bifurcation in the parameter space.

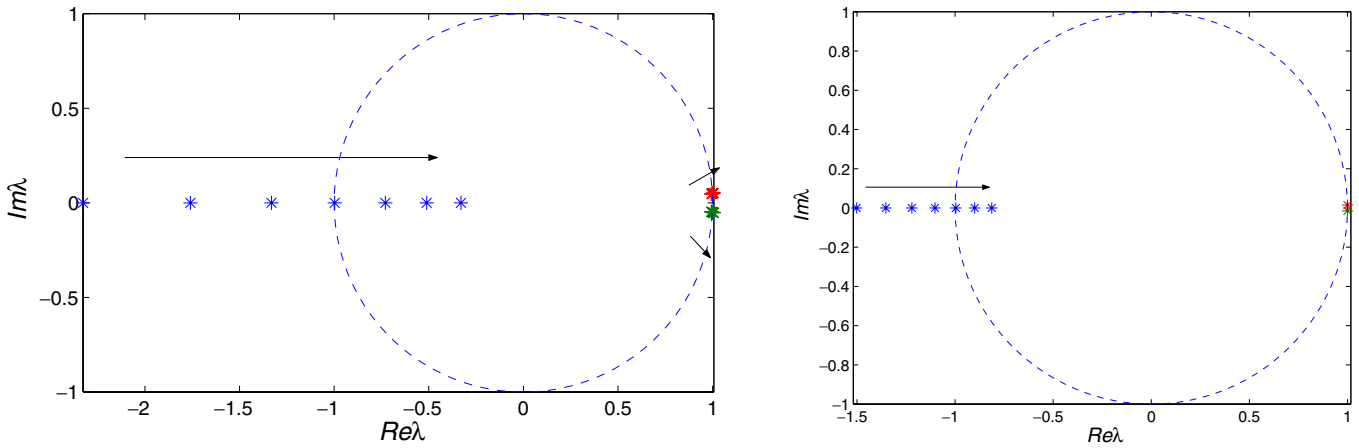

(a) (b)

Fig. 7. Loci of eigenvalues for $E = 6.1877\,\text{V}$, $R = 10.78\,\Omega$ with (a) varying $1/m_1$ when $g = 0.4$ and $\tau_f = 0.8625\,\text{ms}$, (b) varying m_c when $1/m_1 = 31.514 \times 10^{-6}\,\text{s/A}$, $g = 0.4$ and $\tau_f = 1.3253\,\text{ms}$. Arrows indicate the direction of movement of the eigenvalues as the chosen parameters are increased.

5. Application: Derivation of Boundaries of Operations

In this section, we take a detailed look into the qualitative behaviors of the system, and present the boundaries of stable region, slow-scale bifurcation region, fast-scale bifurcation region, and coexisting (interacting) fast and slow-scale bifurcation region in terms of selected circuit parameters. The operation boundaries, as shown in Figs. 8–10, are derived from cycle-by-cycle simulations and the theoretical analysis is discussed in Sec. 4. As mentioned previously, such boundaries of operations provide essential design-oriented information that allows the system parameters to be selected in an informed manner.

5.1. *Effects of varying input voltage E and load resistance R*

The behavior of the system varies with E and R. Two perspectives of operating boundaries are

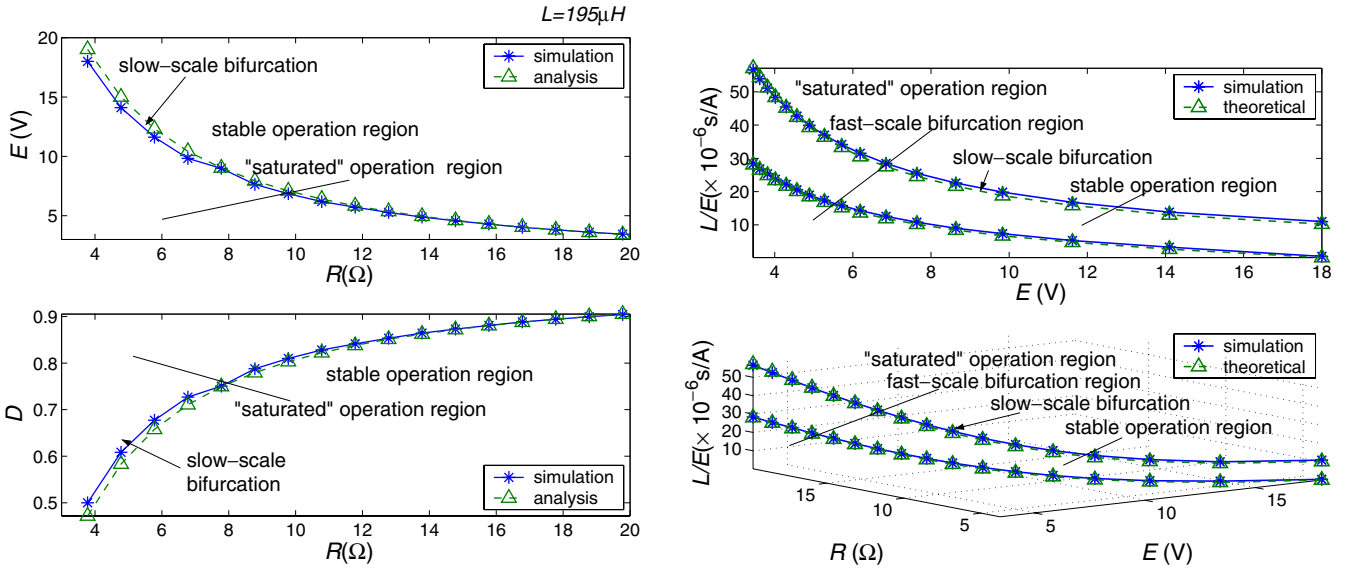

(a) (b)

Fig. 8. Operating boundaries under (a) varying E and D; (b) varying L/E.

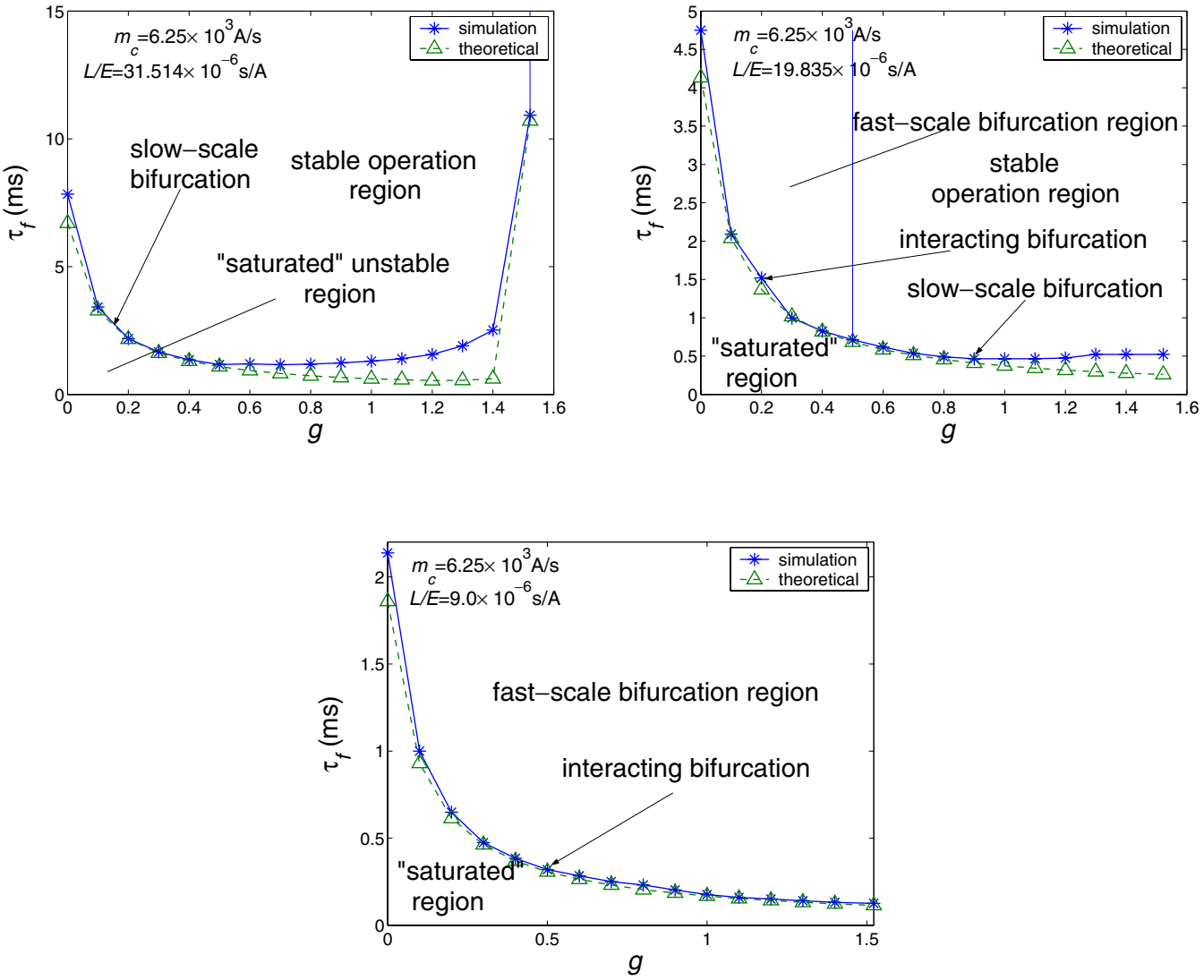

Fig. 9. Operating boundaries under varying feedback gain and time constant for $E = 6.1877\,\mathrm{V}$ and $R = 10.78\,\Omega$.

shown in Fig. 8(a), where the boundaries divide regions of stable operation and "saturated" region. The transition from the stable region to the other is a slow-scale Hopf type bifurcation. Parameters except R and E are kept as listed in Table 1. As shown in Fig. 8(a), the simulated boundaries are completely consistent with the analysis described in the previous section. See Fig. 5(a) for a corresponding illustration of the loci of eigenvalues.

5.2. *Effects of varying rising slope of inductor current E/L*

The rising slope of the inductor current, $m_1 = E/L$, has significant influence on the operation of the system. For each pair of E and R used in the simulation, we choose those points located on the boundary curve in Fig. 8(a), and change L while keeping all other parameters as listed in Table 1. Note that the value of L should be chosen to ensure CCM operation. The simulated operation boundaries are shown in Fig. 8(b) in two perspectives. Note that E/L can be varied by changing either E or L. In order to maintain the desired duty cycle and for convenience of plotting, we only change L and keep E constant. The simulated boundaries are completely consistent with the analysis described in the previous section. See Fig. 5(b) for a corresponding illustration of the loci of eigenvalues.

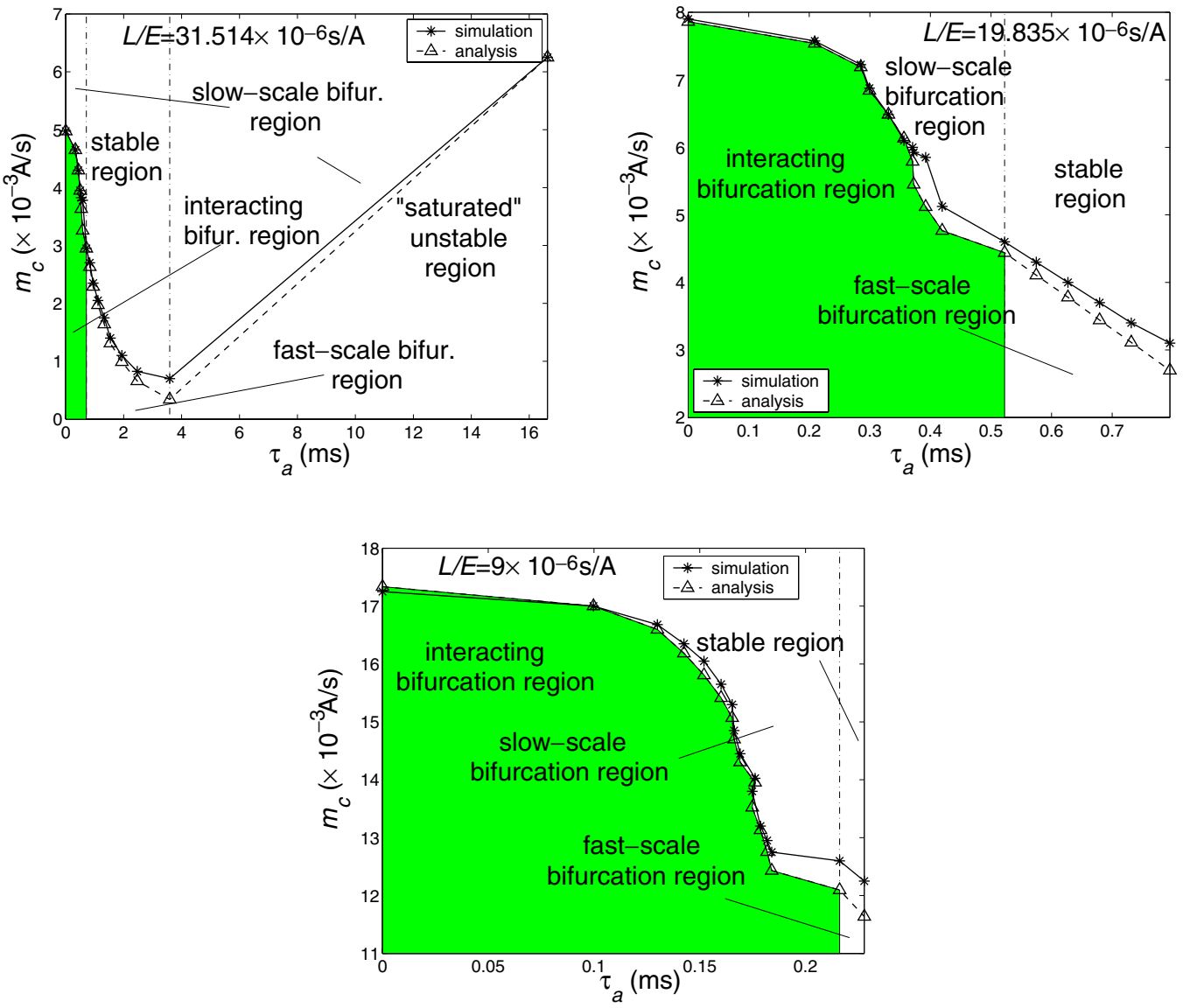

Fig. 10. Operating boundaries with varying compensation slope and $\tau_a = R_a C_a = g\tau_f$.

5.3. *Effects of varying feedback gain g and time constant τ_f*

The feedback gain and time constant have obvious influence on the stability, especially for the slow-scale bifurcation because of the bandwidth limitation imposed by the time constant. We keep E and R constant, and vary L/E. We can then change g and τ_f by varying R_a and C_a. Figure 9 shows the stability boundaries for different values of L/E, corresponding to the slow-scale bifurcation boundary, stable region and fast-scale bifurcation region of Fig. 8(b). In Fig. 9, the regions under the boundary curves corresponds to the "saturated" operation, and the operations above the boundaries depend on the values of L/E and g. As seen from Fig. 9, interacting slow and fast-scale bifurcations can be observed for some parameter ranges corresponding to relatively small L/E. As shown in Fig. 9, the simulated boundaries agree well with those derived from the analysis described in Sec. 4. As examples, corresponding illustrations of eigenvalues when varying g, τ_f and L/E under relative small g and τ_f can be seen in Tables 2–4 and Figs. 6(a), 6(b) and 7(a), respectively.

5.4. *Effects of varying compensation ramp m_c*

It has been known that the compensation ramp strongly affects the instability. Varying m_c will lead to interacting slow and fast-scale bifurcations. In

our simulation, we vary m_c by changing the ramp amplitude V_p. Boundary of operations are plotted in Fig. 10, from which we see clearly that both fast-scale and interacting fast and slow-scale bifurcations are possible. It is worth noting that varying m_c has little effect on slow-scale bifurcation, such as the period of the limit cycle and the amplitude of the low-frequency oscillations, as shown previously in Fig. 4. As shown in Fig. 10, the simulated boundaries are consistent with the analysis described in the previous section. A corresponding illustration of the loci of eigenvalues has been shown earlier in Fig. 7(b) and also in Table 5.

6. Conclusion

In this paper we have studied the interaction of slow and fast-scale bifurcations both by cycle-by-cycle computer simulation and theoretical analysis based on a nonlinear discrete-time model. Basically we have observed that under certain parameter ranges, current-mode controlled boost converters can be fast-scale and slow-scale unstable simultaneously. Such interacting bifurcation occurs when the low-frequency voltage loop and the fast inner current loop become unstable simultaneously. In general, the main parameters affecting fast-scale bifurcations are the rising slope of the inductance current, and the slope of compensation ramp, whereas those affecting slow-scale bifurcations are the voltage feedback gain g and time constant, as studied previously in [Banerjee & Verghese, 2000]. The results in this paper show that the slow-scale bifurcation can be eliminated by decreasing the feedback gain and/or bandwidth, and the readiness of fast-scale bifurcation can be reduced by increasing the slope of the compensation ramp or decreasing the rising slope of the inductor current while keeping the input voltage constant. In this paper, we have identified the parameter ranges under which slow-scale, fast-scale, and interacting slow and fast-scale bifurcations occur for facilitating the design of such converters.

Acknowledgment

This work is supported by Hong Kong Polytechnic University under a Research Grant for Chair Professors (No. 1-BBZA).

References

Banerjee, S. & Chakrabarty, K. [1998] "Nonlinear modeling and bifurcations in the boost converter," *IEEE Trans. Power Electron.* **13**, 252–260.

Banerjee, S. & Verghese, G. (eds.) [2000] *Nonlinear Phenomena in Power Electronics*: *Attractors*, *Bifurcations*, *Chaos and Nonlinear Control* (IEEE Press, NY).

Chan, W. C. Y. & Tse, C. K. [1997] "Study of bifurcations in current-programmed dc/dc boost converters: From quasi-periodicity to period-doubling," *IEEE Trans. Circuits Syst.-I* **44**, 1129–1142.

El Aroudi, A., Benadero, L., Toribio, E. & Oliver, G. [1999] "Hopf bifurcation and chaos from torus breakdown in a PWM voltage-controlled dc-dc boost converter," *IEEE Trans. Circuits Syst.-I* **46**, 1374–1382.

Guckenheimer, J. & Holmes, P. [1983] *Nonlinear Oscillations*, *Dynamical Systems and Bifurcations of Vector Fields* (Springer-Verlag, NY).

Iu, H. H. C. & Tse, C. K. [2001] "Bifurcation behavior in parallel-connected buck converters," *IEEE Trans. Circuits Syst.-I* **48**, 223–240.

Redl, R. & Sokal, N. O. [1985] "Current-mode control, five different types, used with three basic classes of power converters," *IEEE Power Electronics Specialists Conf. Record*, pp. 771–775.

Stjepan, P. & Dragan, M. [1991] "Using a discrete-timemodel for large-signal analysis of a current-programmed boost converter," *IEEE Power Electronics Specialists Conf. Record*, pp. 715–721.

Tse, C. K., Lai, Y. M. & Iu, H. H. C. [2000] "Hopf bifurcation and chaos in a free-running current-controlled Ćuk switching regulator," *IEEE Trans. Circuits Syst.-I* **47**, 448–457.

Wong, S. C., Tse, C. K. & Tam, K. C. [2004] "Intermittent chaotic operation in switching power converters," *Int. J. Bifurcation and Chaos* **14**, 1971–2978.

Wong, S. C., Tse, C. K., Orabi, M. & Ninomiya, T. [2006] "The method of double averaging: An approach for modeling power-factor-correction power converters," *IEEE Trans. Circuits Syst.-I* **53**, 454–462.

Wu, X., Tse, C. K., Dranga, O. & Lu, J. [2006] "Fast-scale instability of single-stage power-factor-correction power supplies," *IEEE Trans. Circuits Syst.-I* **53**, 204–213.